Deciphering China's complex pattern of summer precipitation trends

Mei Li, Chao Li, Zhihong Jiang, Xuebin Zhang, & Francis W. Zwiers

2022

Original citation:

Li, M., Li, C., Jiang, Z., Zhang, X., & Zwiers, F. W. (2022). Deciphering China's complex pattern of summer precipitation trends. *Earth's Future*, *10*(9), e2022EF002797. https://doi.org/10.1029/2022EF002797

Earth's Future

RESEARCH ARTICLE
10.1029/2022EF002797

Deciphering China's Complex Pattern of Summer Precipitation Trends

Mei Li[1,2,3], Chao Li[4,5], Zhihong Jiang[1,2], Xuebin Zhang[6], and Francis W. Zwiers[1,7]

[1]Joint International Research Laboratory of Climate and Environment Change, Key Laboratory of Meteorological Disaster of Ministry of Education, Nanjing University of Information Science and Technology, Nanjing, China, [2]Collaborative Innovation Center on Forecast and Evaluation of Meteorological Disaster, Nanjing University of Information Science and Technology, Nanjing, China, [3]Now at National Climate Center, China Meteorological Administration, Beijing, China, [4]Key Laboratory of Geographic Information Science, Ministry of Education, East China Normal University, Shanghai, China, [5]School of Geographic Sciences, East China Normal University, Shanghai, China, [6]Climate Research Division, Environment and Climate Change Canada, Toronto, ON, Canada, [7]Pacific Climate Impacts Consortium, University of Victoria, Victoria, BC, Canada

Key Points:

- Summer rainfall trends are decomposed into contributions from changes in synoptic pattern frequency, rainfall frequency, and intensity
- There is clear evidence of intensification of precipitation, which is consistent with warming
- The enigmatic "north-south drying-wetting" pattern of summer rainfall in eastern China is the result of changes in rainfall frequency

Supporting Information:

Supporting Information may be found in the online version of this article.

Correspondence to:

C. Li and Z. Jiang,
cli@geo.ecnu.edu.cn;
zhjiang@nuist.edu.cn

Citation:

Li, M., Li, C., Jiang, Z., Zhang, X., & Zwiers, F. W. (2022). Deciphering China's complex pattern of summer precipitation trends. *Earth's Future*, *10*, e2022EF002797. https://doi.org/10.1029/2022EF002797

Received 24 MAR 2022
Accepted 4 AUG 2022

Abstract Observations show that summer precipitation in China has undergone pronounced changes, resulting in an enigmatic "north-south drying-wetting" pattern in eastern China that is of great concern for socio-economic development. Scientific consensus on the mechanisms that are responsible for this pattern of change has not yet been achieved. We show that this complex pattern of summer total precipitation trends observed in China since the 1960s is overwhelmingly the result of changes in daily precipitation frequency, rather than being the result of changes in precipitation intensity or the frequency of synoptic circulation patterns favorable to precipitation. Changes in precipitation intensity, which are very likely due to anthropogenic greenhouse gas forcing, contribute a relatively homogeneous wetting tendency across the country while changes due to synoptic circulation change are weak. The changes in daily precipitation frequency that drive the observed patterns of change may be due to aerosols, but improved process understanding will be required to resolve that question and enable reliable projections of regional scale precipitation change in China and elsewhere.

Plain Language Summary The spatial distribution of summer precipitation has changed substantially in China since the 1960s, creating considerable concern for agriculture and other sectors dependent on summer rainfall. There is currently a lack of scientific consensus on the mechanisms that are responsible for the observed drying-wetting pattern, in part because most studies have considered a single mechanism amongst several that may be responsible. We, therefore, partition summer precipitation trends into three components associated with changes in daily precipitation frequency, daily precipitation intensity, and synoptic circulation pattern (CP) frequency, each corresponding to a different mechanism of change. By doing so we find that China's complex pattern of summer precipitation change is mainly the result of changes in daily precipitation frequency that are layered on top of a widespread increase in precipitation intensity. We argue that the latter is consistent with the effects of human-induced warming. Eliminating changes in precipitation intensity and CP frequency as the causes of the observed pattern of increases and decreases indicates that the primary focus of research should now shift to an understanding of the causes of observed changes in precipitation frequency.

1. Introduction

The Intergovernmental Panel on Climate Change has removed any doubt about the causes of global warming in its Sixth Assessment Working Group I report and has stated that human-induced climate change has affected every region across the globe (IPCC, 2021). Despite such certainty, our understanding of the causes of observed precipitation change at regional scales remains very limited. Observed change in summer precipitation in China is a case in point. China is the third largest country in size in the world, hosts one-fifth of the world population and is highly dependent on summer precipitation because it provides more than half of the annual total precipitation in many regions of the country. Summer precipitation has increased in southern and northwestern regions since the 1960s when systematic observations were established but has decreased elsewhere, resulting in an enigmatic "north-south drying-wetting" pattern in eastern China (Figure 1a) that raises concerns about the sustainability of agricultural production and water-dependent socio-economic development (Piao et al., 2010).

10.1029/2022EF002797

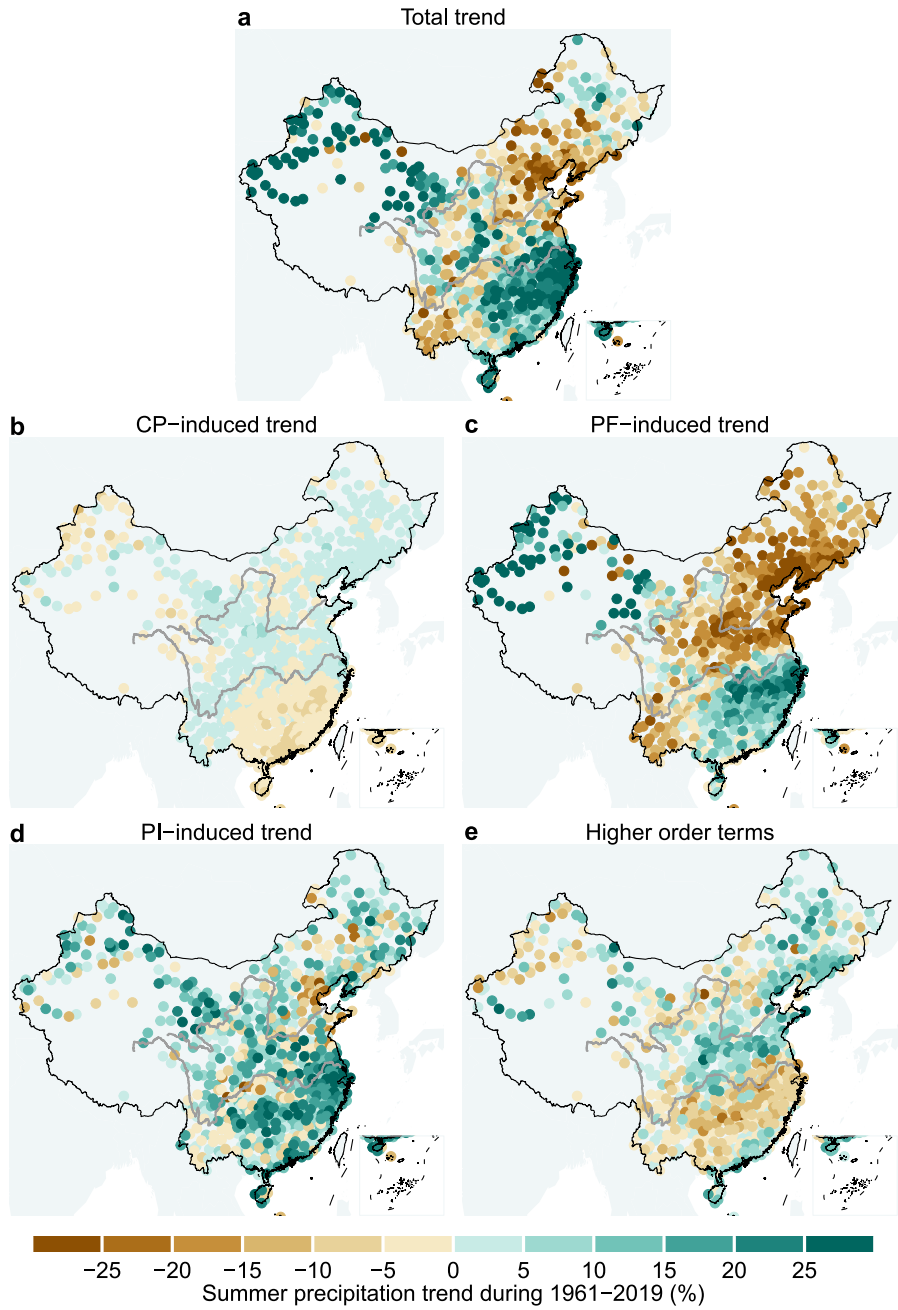

Figure 1. The partition of the 1961–2019 trends in summer total precipitation in China. Panels show (a) the observed trends in summer total precipitation and their partitions into contributions from changes in (b) synoptic circulation pattern frequency, (c) daily precipitation frequency, (d) daily precipitation intensity, and (e) high-order terms due to the interactions of changes in two or more of the three components. Trends are expressed as percentage changes during the whole 1961–2019 period relative to the climatological mean summer total precipitation of that period.

A key question for adaptation in densely populated eastern China is to know whether this pattern will continue into the future, which requires careful interpretation of the causes of this observed pattern of change. Mechanisms that have been proposed to explain this pattern are wide ranging and thus reflect that scientific consensus has not yet been achieved. These mechanisms include natural internal variability (e.g., Ding et al., 2008; Gong & Ho, 2002; R. Zhang, 2015), anthropogenic changes in aerosols (e.g., Menon et al., 2002; Polson et al., 2014; Tian et al., 2018; L. Zhang et al., 2017), and changes in the frequency of synoptic circulation patterns (CPs; B. Zhou et al., 2020; B. Zhou, Zhai, et al., 2021). Seasonal precipitation can, however, be modulated by the frequency

and intensity of daily precipitation events, both of which are further affected by the occurrence of synoptic CPs favorable to precipitation (e.g., Chou et al., 2012; Driouech et al., 2010; Prein et al., 2016; Y. Tan et al., 2020; B. Zhou et al., 2020). As climate warms, precipitation intensity is expected to increase and precipitation frequency is expected to decrease on average over the globe or a large domain (e.g., Dai et al., 2020; Sun et al., 2007; Trenberth et al., 2003), as has also been observed in China (Lu et al., 2014; Ma et al., 2015; Zhai et al., 2004). Observed changes may be due to both thermodynamic responses to external forcing and the dynamic effects of either external forcing or natural low-frequency variability. We will demonstrate that simultaneously considering changes in precipitation frequency, precipitation intensity, and dynamical factors can help clarify the causes of the observed changes in seasonal precipitation in a region such as China with complex monsoon circulation influences.

At the regional scale, dynamical influences on precipitation can be characterized through the frequency of occurrence of synoptic CPs that are favorable to precipitation (e.g., Driouech et al., 2010; Prein et al., 2016; Y. Tan et al., 2020; B. Zhou et al., 2020). We, therefore, classify synoptic CPs affecting China in summer into several types, and represent the annual summer (June–August) wet-day precipitation amounts in China associated with the occurrence of each pattern as the product of the frequency and intensity of daily precipitation conditional on that synoptic CP. This in turn allows, for the first time, a successful decomposition of long-term trends in total summer precipitation into three components associated with changes in synoptic pattern frequency, precipitation frequency, and precipitation intensity. In contrast, previous studies accounting for synoptic circulation variations seem to have invariably considered their impacts on changes in precipitation averages over both wet and dry days, in which the effects of changes in precipitation frequency and intensity are convolved together.

The decomposition allows us to demonstrate that the complex pattern of summer total precipitation trends observed in China since the 1960s is overwhelmingly the result of changes in daily precipitation frequency. Changes in precipitation intensity contribute a relatively homogeneous wetting tendency across the country and, in contrast with previous studies (e.g., B. Zhou et al., 2020; B. Zhou, Zhai, et al., 2021), changes due to synoptic circulation change are found to be weak. Our partition of seasonal precipitation trend into components that reflect the processes controlling precipitation occurrence and intensity helps establish a pathway for understanding how human activities have influenced China's summer precipitation by identifying human fingerprints in the individual components.

2. Methods and Data

2.1. Classification of Synoptic Circulation Patterns

The classification of synoptic CPs is performed by self-organizing map analysis (Kohonen, 2000) of daily mean 500 hPa geopotential height and sea level pressure from the latest European Center for Medium-Range Weather Forecasts reanalysis v5 (ERA5; Hersbach et al., 2019) during the summers of 1961–2019 within the boundaries 40°–160° east and 0°–70° north. These two variables have also been used in previous studies for classifying CPs affecting summer precipitation in China (e.g., B. Zhou et al., 2020, B. Zhou, Zhai, et al., 2021). As will be seen later, they capture the key CPs (Figure 2) relevant to large-scale anomalous precipitation centers (Figure 3), which appropriately reflect the seasonal march of precipitation in eastern China in response to the progression of the East Asian summer monsoon (e.g., Ding et al., 2008). The choice of self-organizing map analysis is motivated by its unique advantage over other synoptic typing approaches in conserving the topology of the input circulation fields during classification, thus producing smoothly transitioning CPs (e.g., Hewitson & Crane, 2002), which are particularly important for capturing CPs responsible for the above-mentioned seasonal march of monsoon related precipitation belt.

To remove the effect of the atmospheric warming-induced expansion of the troposphere in the increase of geopotential height (Figure S1 in Supporting Information S1), we subtract the area-weighted average daily geopotential height over the study domain from the raw values (e.g., Driouech et al., 2010; He et al., 2015), maintaining the horizontal gradients of the raw fields that control the large-scale atmospheric circulation in the mid-latitudes. We then normalize the resulting eddy geopotential height and sea level pressure by subtracting their means at individual grid cells and dividing by their standard deviations, both calculated using data for the whole 1961–2019 period.

Although various sources of satellite observations have been assimilated into the reanalysis post 1978, the introduction of satellite data does not appear to have caused a discernible shift in the occurrence frequency of the

10.1029/2022EF002797

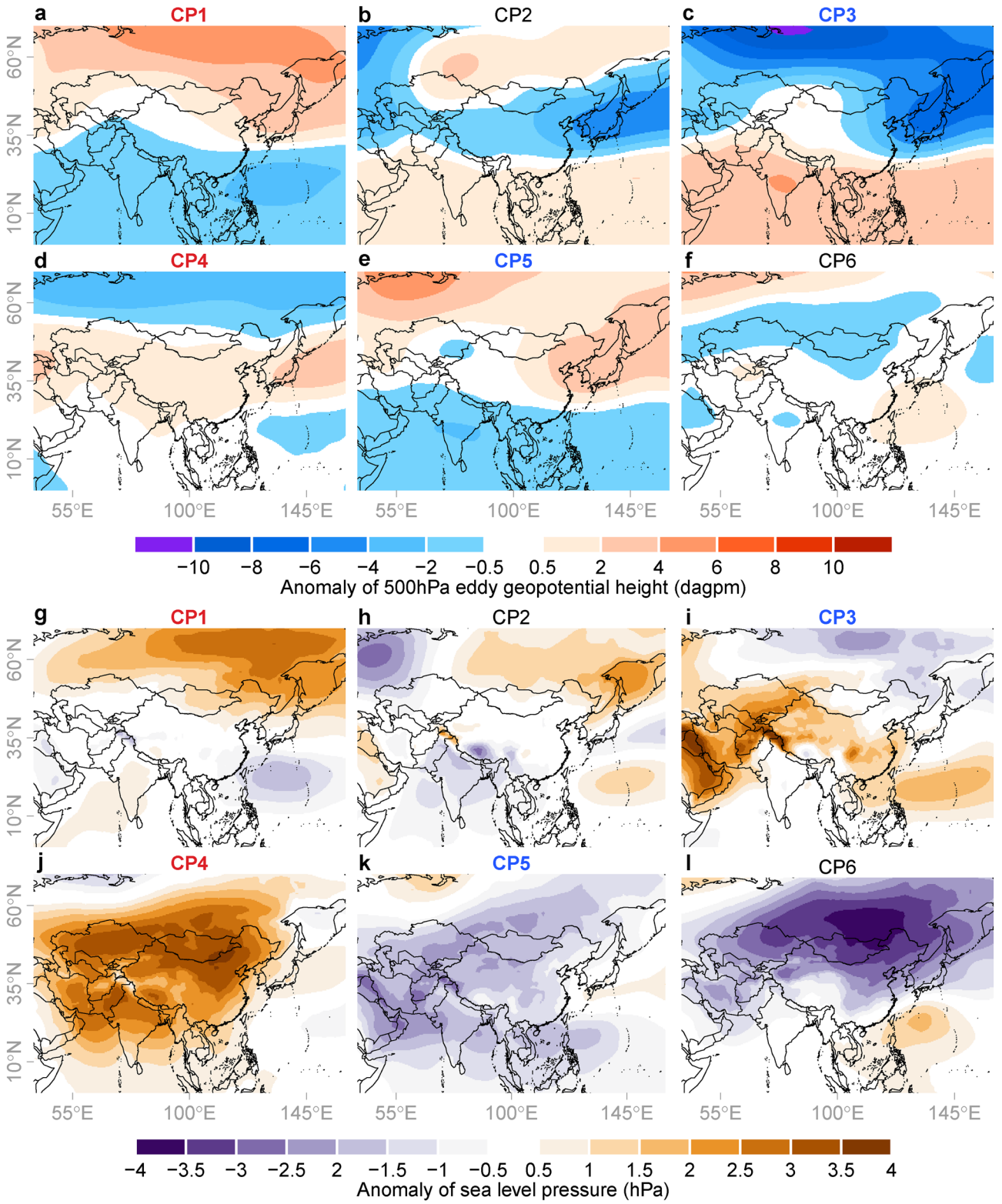

Figure 2. Dominant summer synoptic circulation patterns over China. The synoptic circulation patterns are represented by anomaly patterns of (a–f) 500 hPa eddy geopotential height and (g–l) sea level pressure as identified by self-organizing map analysis of the ERA5 reanalysis of the two atmospheric variables. Synoptic circulation patterns showing statistically significant increasing and decreasing tendencies at a significance level of 5% are marked by red and blue labels, respectively.

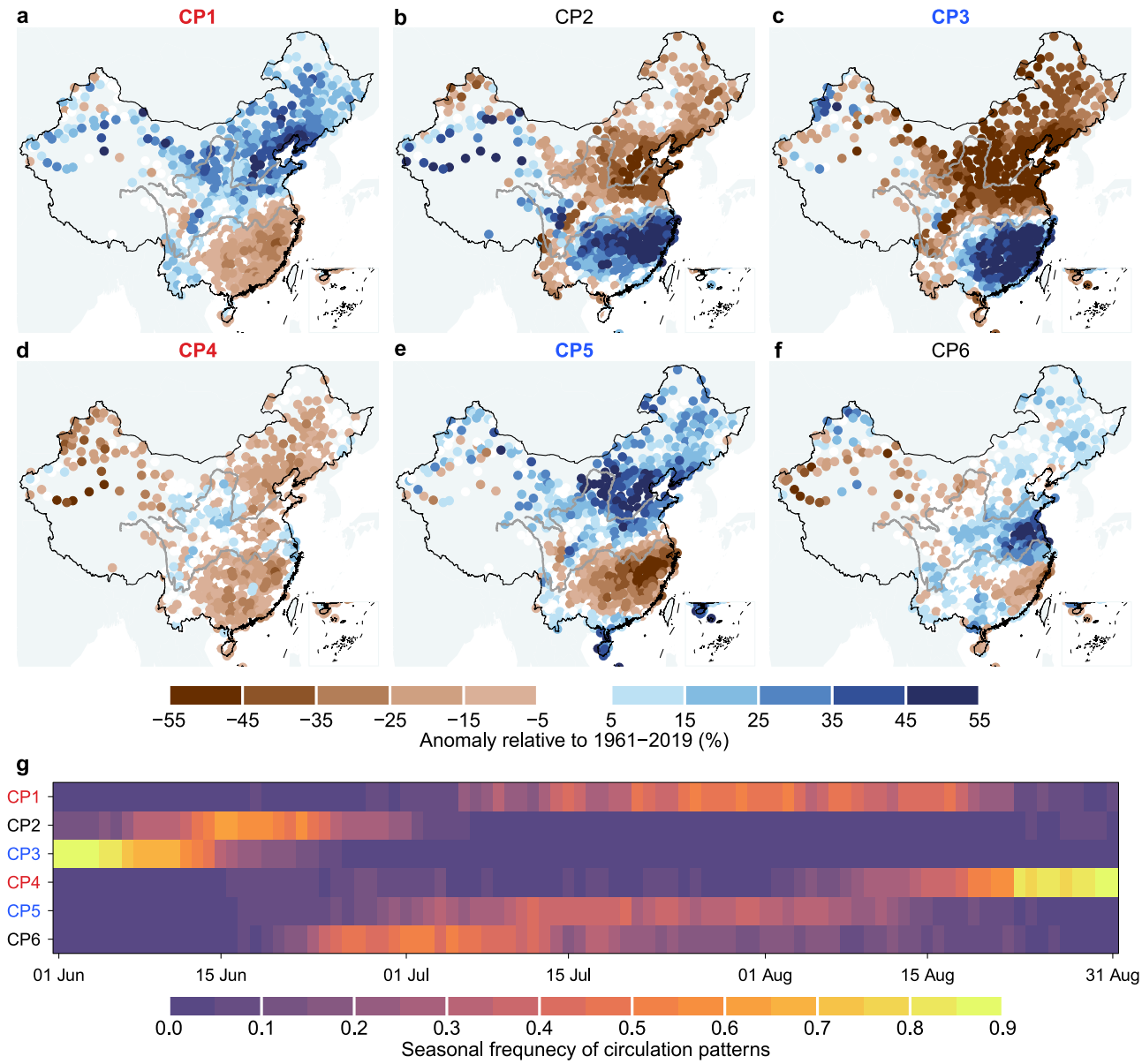

Figure 3. Precipitation patterns associated with the dominant synoptic circulation patterns and their seasonal occurrence frequencies. (a–f) Top panels show the mean percentage anomalies of precipitation over days within each circulation pattern relative to 1961–2019. (g) The bottom panel shows the 1961–2019 climatological mean occurrence frequencies of these precipitation patterns in calendar days during summer. Synoptic circulation patterns showing statistically significant increasing and decreasing tendencies at a significance level of 5% are marked by red and blue labels, respectively.

classified CPs (black lines in Figure 4). As will be discussed, our major findings are robust to the use of the Japanese 55 yr reanalysis (JRA55; Kobayashi et al., 2015) as well as to the removal of the thermal expansion of geopotential height by subtracting the domain average seasonal mean trend (Cattiaus et al., 2013; Figure S2 in Supporting Information S1).

The self-organizing map clusters the daily fields of 500 hPa eddy geopotential height and sea level pressure into a two-dimensional array of nodes (i.e., CPs) through an iterative training process. At each iteration, a daily field is randomly chosen and presented to the current node array to find the so-called "winning" node that is closest to the input field according to the Euclidean distance. The winning node and its neighboring nodes are updated such that the winning node is more similar to the input field while simultaneously all nodes keep similar to their neighbors. This process is repeated until there is no further appreciable change in the nodes.

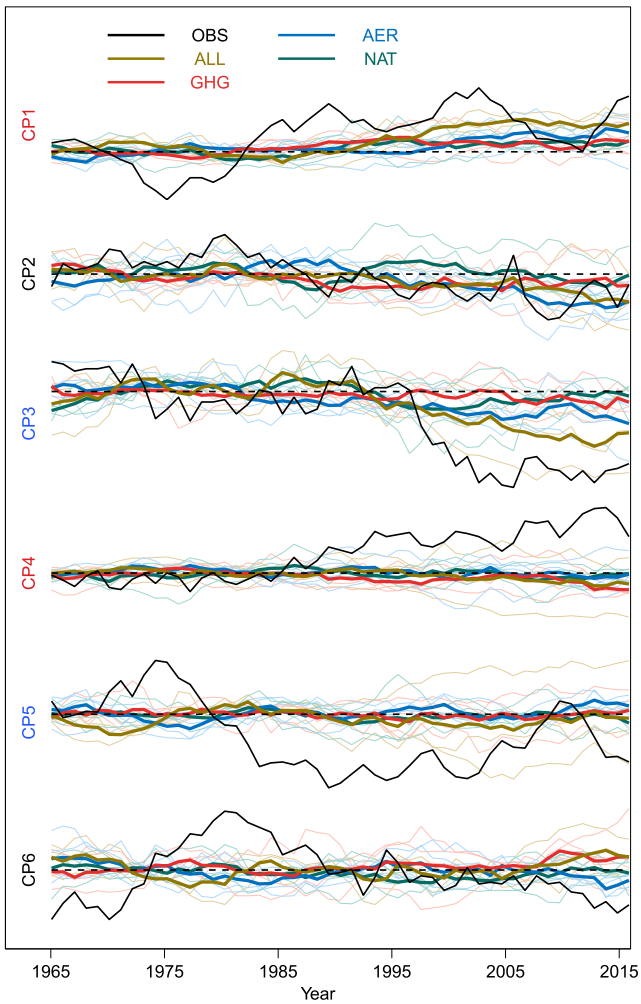

Figure 4. Comparison of circulation pattern frequencies in ERA5 reanalysis and global climate model simulations. The 5 yr running mean occurrence frequencies of the dominant summer synoptic circulation patterns during 1961–2019 from ERA5 reanalysis (back lines) and those derived from ALL-forcing (brown lines), greenhouse gas forcing only (red lines), aerosol forcing only (blue lines), and natural external forcing only (green lines) climate simulations from the available CMIP6 climate models that simultaneously have at least three simulations for each of the forcings considered (CanESM5, FGOALS-g3, MIRCO6, and MRI_ESM2-0). Thick lines show the multi-model mean frequencies and thin lines show the frequencies of individual models. Synoptic circulation patterns in ERA5 showing statistically significant increasing and decreasing tendencies at a significance level of 5% are marked by red and blue labels, respectively.

The extent to which nodes can be updated from one iteration to the next is controlled by a learning rate parameter, which is set to decline linearly from 0.05 to 0.01 through the training process. The neighboring nodes are identified according to a neighborhood radius parameter, which is set to initially cover 2/3rds of the nodes in the node array and gradually reduces such that eventually only the winning nodes are updated. We confirmed that the classified CPs are not sensitive to these parameter settings for a given node array, as was also discussed in a number of previous studies (e.g., Horton et al., 2015; X. Tan et al., 2019, Y. Tan et al., 2020).

The size of the node array (or dominant CPs) to be classified, which has to be specified prior to the learning process, should be sufficient to capture a wide range of CPs while avoiding the identification of overly similar patterns (Horton et al., 2015; Y. Tan et al., 2020). By analyzing a number of node arrays (i.e., 1×3, 2×3, 3×3, 3×4, 4×4, 4×5), we find that the choice of node array does not strongly affect the estimates of summer precipitation trends associated to changes in CPs (Figure S3 in Supporting Information S1). We, therefore, base our analysis in the main text on a moderate 2×3 node array for simplicity of presentation.

2.2. Evaluation of Changes in Synoptic Circulation Pattern Frequency

Once the CPs are classified, we count the total number of active days for each pattern in each summer and determine whether the occurrence frequencies of the CPs have changed significantly. We find that, even with the relatively small 2×3 node array, some CPs did not occur in some years (not shown), challenging the evaluation of their frequency trends by the linear least squares regression. Previous studies have therefore resorted to approaches such as data transformation (Horton et al., 2015) and generalized linear regression with a Poisson distribution (Furrer et al., 2010; Zhai et al., 2004). To reduce dependence on the assumptions required for such approaches, we evaluate only whether there is an overall increasing or decreasing tendency by using the nonparametric Mann-Kendall test (at a significance level of 5%; Kendall, 1975; Mann, 1945). This test is more robust than other methods that require assumptions that may not be fully satisfied in applications to, for example, time series of CP frequency with scattered zeros (J. Wang et al., 2021).

2.3. Partition of Summer Total Precipitation Trend

For each summer, days are classified according to CPs. Then, for a given summer t, the total precipitation received on wet days under a given CP i is equal to the product of the season length in days, the fraction of wet days, and the wet-day mean precipitation intensity under the given CP i, that is:

$$\Pr(t)_{\mathrm{CP}=i} = F_{\mathrm{CP}=i}(t) P_{\mathrm{CP}=i}(t) I_{\mathrm{CP}=i}(t) \quad (1)$$

where $F_{\mathrm{CP}=i}(t)$ is the occurrence frequency (in days) of CP i in summer t, $P_{\mathrm{CP}=i}(t)$ is the proportion of wet days over all days under CP i in summer t, and $I_{\mathrm{CP}=i}(t)$ is the mean precipitation intensity over wet days under CP i in summer t. Assuming there are n prevailing CPs, the summer total wet-day precipitation can be obtained by summing up $\Pr(t)_{\mathrm{CP}=i}$ for all CPs, that is, by calculating:

$$\Pr(t) = \sum_{i=1}^{n} F_{\mathrm{CP}=i}(t) P_{\mathrm{CP}=i}(t) I_{\mathrm{CP}=i}(t) \quad (2)$$

Here, we consider a day as wet if the accumulated precipitation over that day is greater than 1 mm, as motivated from observational constraints that make small precipitation amounts particularly difficult to measure and thus subject to large uncertainty (e.g., Schär et al., 2016).

The time series of summer total wet-day precipitation anomalies relative to a reference period can be then approximated as:

$$\delta \mathrm{Pr}(t) \approx \sum_{i=1}^{n} \overline{P}_{\mathrm{CP}=i}\, \overline{I}_{\mathrm{CP}=i} \delta F_{\mathrm{CP}=i}(t) + \sum_{i=1}^{n} \overline{F}_{\mathrm{CP}=i}\, \overline{I}_{\mathrm{CP}=i} \delta P_{\mathrm{CP}=i}(t) + \sum_{i=1}^{n} \overline{F}_{\mathrm{CP}=i}\, \overline{P}_{\mathrm{CP}=i} \delta I_{\mathrm{CP}=i}(t) \tag{3}$$

where overbars indicate climatological mean values over the reference period and δ indicates anomalies relative to climatological mean values. Here, we take the whole 1961–2019 study period as the reference period. See Section S1 in Supporting Information S1 for the derivation of this equation.

The three parts on the right-hand side of Equation 3 describes variations of the summer total wet-day precipitation due respectively to (a) CP frequency when precipitation frequency and intensity are assumed constant over days in each CP, (b) precipitation frequency when CP frequency and precipitation intensity are assumed constant for each CP, and (c) precipitation intensity when CP frequency and precipitation frequency are assumed constant for each CP. Variations related to all other higher order terms combined where two or more of these three factors vary jointly, which can be obtained as residuals from the right-hand side of Equation 3, are generally modest. We note that the three first order terms collectively represent more than 90% of the interannual variance in summer total wet-day precipitation (Figure S4 in Supporting Information S1).

Based on the CPs identified from the ERA5 reanalysis, we use Equation 2 to partition summer daily precipitation observed at 726 meteorological stations located across mainland China (except the Tibetan plateau, where virtually no observations exist; see Figure 1 for station locations). These observations, obtained from the National Meteorological Information Center of China, have been homogenized to reduce possible influences due to station relocation and changing measurement instruments (Z. Li et al., 2015) and have fewer than 10 missing values per summer in the study period. For each station, we estimate trends in the three precipitation components using nonparametric Sen's slope estimator (Sen, 1968). Trend estimates are expressed as percentage changes over the 1961–2019 period relative to the climatological mean summer total precipitation of that period.

2.4. Detection and Attribution Analysis on Synoptic Circulation Change

To study whether human activity has altered synoptic circulations relevant to summer precipitation in China, we conduct a set of optimal fingerprinting analyses on CP frequency during 1961–2019 as identified from the ERA5 reanalysis. We use simulations of daily 500 hPa geopotential height and sea level pressure for the 1961–2019 period from Phase 6 of the Coupled Model Intercomparison Project (CMIP6; Eyring et al., 2016) climate models with at least three ensemble members for anthropogenic and natural forcings (ALL), anthropogenic greenhouse gases forcing only (GHG), anthropogenic aerosols forcing only (AER), and natural forcing only (NAT). The historical ALL simulations, if they end at the year 2014, were extended to 2019 using Shared Socioeconomic Pathway 2–4.5 simulations (Meinshausen et al., 2020).

Four climate models have the necessary simulations: CanESM5, FGOALS-g3, MIROC6, and MRI_ESM2_0. We converted the simulations to the ERA5 resolution using bilinear interpolation and processed each as for the ERA5 reanalysis, including the calculation of eddy geopotential height to account for the effect of thermal tropospheric expansion. The normalized simulations are projected onto the reanalysis CPs based on their Euclidean distance to the patterns. The frequencies of the CPs for all summers in the simulations are calculated and converted to anomalies relative to 1961–1990, which are then used to estimate the forced responses of CP frequency to ALL, GHG, AER, and NAT forcings by averaging the corresponding simulations that are available in each model and then calculating the mean of the model averages.

The optimal fingerprinting analysis regresses the reanalysis CP frequency $\boldsymbol{Y}$ onto the simulated responses to sets of external forcings $\boldsymbol{X}_i$ using the regularized total least squares algorithm (Allen & Stott, 2003; Ribes et al., 2013) as follows:

$$\boldsymbol{Y} = \sum_{i} \beta_i \boldsymbol{X}_i^{*} + \boldsymbol{\varepsilon}_Y \tag{4}$$

$$\boldsymbol{X}_i = \boldsymbol{X}_i^* + \epsilon_i \quad (5)$$

where $\boldsymbol{Y}$ is the vector of non-overlapping 5 yr mean anomalies of reanalysis CP frequencies from 1961–1965 to 2016–2019 (with the last 5 yr period consisting of 4 yr); $\boldsymbol{\epsilon}_Y$ represent unforced internal variability in $\boldsymbol{Y}$; $\boldsymbol{X}_i$ is an estimate of the true model response $\boldsymbol{X}_i^*$ subject to model internal variability error ϵ_i. CP frequencies derived from the preindustrial control simulations of all available CMIP6 climate models with output of daily 500 hPa geopotential height and sea level pressure (AWI_ESM_1_1_LR, CanESM5, CESM2, CESM2_FV2, CESM2_WACCM, EC_Earth3, EC_Earth3_LR, HadGEM3_GC31_MM, IITM_ESM, INM_CM5_0, MPI_ESM1_2_HR, and MRI_ESM2_0) are used to estimate the covariance matrix of internal variability for optimizing the fingerprinting regression. Detection and attribution inferences are made with the estimated regression coefficients β_i. The response to forcing i is detected if β_i is statistically non-zero at a significance level of 10%, while if it is simultaneously indistinguishable from one, the reanalysis CP frequency change may be attributable to forcing i.

We consider three different 2-signal fingerprinting analysis configurations involving ALL and NAT responses, ALL and GHG responses, and ALL and AER responses, respectively. The first configuration serves to detect the influence of anthropogenic forcing (ANT) that combines GHG and AER while accounting for the NAT influence. The other two configurations further assess whether the individual influences of GHG and AER are detectable in the presence of other forcings (denoted by OGHG and OAER), respectively. As one of the two forcing responses of interest is not explicitly included in these fingerprinting regressions, such as the ANT response in the ALL + NAT configuration, we derive the needed regression coefficients by linear transformations of regression coefficients for the responses explicitly included (e.g., C. Li, Wang, et al., 2021). We conduct both separate analyses for individual CPs and joint analyses including all CPs in the same fingerprinting regression except the pattern showing no tendency of change to ensure valid estimates of the covariance matrix of the estimated responses. As will be seen in the following section, there are two such CPs. Excluding either pattern, or even both, from the joint fingerprinting analysis does not qualitatively change the presented detection and attribution conclusions (not shown).

3. Results

3.1. Synoptic Circulation Patterns During Summer in China

The dominant synoptic CPs during the 1961–2019 summers as represented in the ERA5 reanalysis are presented in Figure 2. These CPs correspond well to distinctly different spatial patterns of precipitation (Figure 3). For instance, the CP labeled by CP1 has a weakened meridional eddy 500 hPa geopotential height gradient (Figure 2a) and low sea level pressure over the northwestern Pacific (Figure 2g), which strengthens moisture divergence (Figure S5 in Supporting Information S1) and drying (Figure 3a) over southern China. In contrast, the CP labeled by CP3 exhibits an enhanced meridional eddy 500 hPa geopotential height gradient with an anomalous trough over the Japan Sea (Figure 2c) and high sea level pressure to the east of the Philippines (Figure 2i), producing a precipitation pattern that is roughly opposite to that associated with CP1 (Figure 3c).

The mean seasonal occurrences of these CPs and associated precipitation patterns capture the typical seasonal march of summer precipitation in eastern China in response to the progression of the East Asian summer monsoon (Figure 3). When CP3 prevails in the first half of June (Figure 3g), which is around the last stage of the pre-flood season in southern China, rainfall is restricted to this region (Figure 3c). Then, from mid-June to mid-July, CP2 and CP6 become active and the rain belt moves northward to the middle and lower reaches of the Yangtze River (Figure 3b) and the Huai River Basin (Figure 3f). This period coincides with the well-known "Meiyu season"; the associated Meiyu trough can be seen clearly at 500 hPa in CP2 (Figure 2b). From mid-July to mid-August, CP5 and CP1 start to stand out in sequence, and with the rain belt advancing further northward (Figures 3a and 3e). Subsequently, the CP4 pattern governs dry anomalies that occur almost everywhere in the country except part of western China and the east coast (Figure 3d), which marks the last stage of rainy season associated with the East Asian summer monsoon.

The correspondence between the circulation and precipitation patterns and their success in capturing the seasonal march of precipitation in eastern China provides physical justification for evaluating the relationship between the observed trends in summer total precipitation and changes in the frequency of occurrence of the CPs. These frequencies have exhibited substantial variations over the 1961–2019 period (black lines in Figure 4), with some

showing statistically significant increases or decreases (i.e., the CP1, CP3, CP4, CP5 patterns). In particular, the increased frequency of CP4 and decreased frequency of CP5, which correspond to anomalous northerly and southeasterly winds over the monsoon region in China (Figure S5 in Supporting Information S1), are consistent with the extensively discussed large-scale weakening of the East Asian summer monsoon since the end of the 1970s (e.g., Ding et al., 2008; Gong & Ho, 2002; Menon et al., 2002; Polson et al., 2014; Tian et al., 2018; L. Zhang et al., 2017; R. Zhang, 2015).

3.2. Drivers of Summer Total Precipitation Change in China

The trends in summer total wet-day precipitation related to changes in CP frequencies obtained from the first component of the decomposition in Equation 3 are rather weak throughout the country (Figure 1b). This finding is insensitive to whether we use ERA5 or the JRA-55 reanalysis (Figure 1 vs. Figure S6 in Supporting Information S1) and to the number of classified CPs (Figure S3 in Supporting Information S1). This suggest that the spatial structure of the observed trends in summer total precipitation, including the "north-south drying-wetting" pattern in eastern China, is not primarily due to changes in the occurrence frequencies of synoptic CPs.

But then, what does drive the relatively complex spatial structure of the observed trends? Trends related to changes in the frequency of daily precipitation obtained from the second component of the decomposition in Equation 3 have a spatial pattern that is in surprisingly good agreement with the observed trends in summer total precipitation (Figure 1c vs. Figure 1a), with a pattern correlation of ∼0.8. Regardless of region, negative trends associated with changes in precipitation frequency arise from decreases in the number of light precipitation days that have precipitation accumulations less than 10 mm/day (Figure S7 in Supporting Information S1). Positive trends, on the other hand, have a somewhat more complex origin, with those in northwest China resulting from increases in the frequency of light precipitation days, and those in south China resulting mainly from increases in heavy precipitation days with accumulations greater than 50 mm/day (Figure S7 in Supporting Information S1).

Trends related to changes in daily precipitation intensity obtained from the third component of the decomposition in Equation 3 do not contribute to the observed drying-wetting pattern. These trends are almost consistently positive and relatively homogeneous in space, with a slight amplification in the lower reaches of the Yangtze River. The country median value of these trends expressed as a proportion of summer total wet-day precipitation is ∼7.5%. Adding the trends associated with changes in precipitation intensity to those associated with changes in precipitation frequency results in combined estimates that, to first order, can be thought of as arising from changes in precipitation properties. We find that these estimates explain most of the observed total precipitation trends, with a pattern correlation of ∼0.9. In summary, the observed trends in summer total precipitation in China are predominately contributed by changes in daily precipitation frequency and intensity (conditional on synoptic patterns), particularly the former, which is the source of the complex spatial structure of the observed trends.

The trends in the combination of higher order terms (Figure 1e), which are dominated by the interaction of changes in CP frequency and precipitation occurrence (see Section S1 and Figuree S8 in Supporting Information S1) tend to be substantially weaker than the trends in the precipitation frequency and intensity components of the decomposition. Moreover, it is worth noting that these trends oppose, or modulate, the effect of the change in precipitation frequency in inducing the observed "north-south drying-wetting" pattern.

3.3. Linking Trend Components to External Forcing

The above trend partition suggests that an improved understanding of the influence of human-induced climate change on summer total precipitation in China can be gained by considering the impact of external forcing on the individual trend components. We begin by considering CP frequency changes, that is, changes in $F_{CP=i}(t)$ in Equation 2, and whether they are related to low-frequency internal climate variability. A correlation analysis reveals that variations in the CP frequencies are not strongly connected with the detrended large-scale climate indices representing typical modes of natural internal climate variability, such as El Niño Southern Oscillation, North Atlantic Oscillation, Pacific Decadal Oscillation, or Atlantic Multi-decadal Oscillation (Figure S9 in Supporting Information S1), consistent with a previous finding but in North America (Prein et al., 2016). This implies that the synoptic circulation changes that have contributed to the "north-south wetting-drying" tendency in eastern China (Figure 1b) are not likely a signature of teleconnected low-frequency internal climate variability and

suggests instead the possibility that these changes reflect the impacts of external forcing, for example, as a consequence of Hadley cell expansion due to anthropogenic global warming (Grise & Davis, 2020; Kim et al., 2017).

Nevertheless, formal fingerprinting analyses show that the signals of anthropogenic greenhouse gases, aerosols, or their combination are not robustly detectable in the reanalysis CP frequencies (i.e., changes in $F_{CP=i}(t)$ in Equation 2; not shown). The climate models we used in the fingerprinting analyses (restricted to CanESM5, FGOALS-g3, MIRCO6, and MRI_ESM2-0 because they have the necessary output) reproduce reasonably well the spatial structures of the reanalysis CPs (Figure S10 vs. Figure S11 in Supporting Information S1) and their climatological mean frequencies during the 1961–2019 study period (Figure S12 in Supporting Information S1), in line with previous findings that global climate models can well capture the climatology of East Asia summer monsoon circulations (e.g., Song & Zhou, 2014). The models, however, do not simulate trends in these CP frequencies during the study period regardless of external forcing (Figure 4), suggesting either poor climate model skill in simulating the effects of external forcing on CP frequency or that the synoptic circulation itself does not respond strongly to external forcing during the study period and that the reanalysis contains spurious changes in CP frequency. Overall, further evidence is required to determine whether human influence on summer synoptic circulation has become discernible, although one recent study that did not account for tropospheric thermal expansion has made such a link (T. Zhou, Ren, et al., 2021). We obtain a similar result when not accounting for thermal expansion (Figures S13–S14 in Supporting Information S1), which is necessary to avoid confounding the thermal responses to external forcing with its dynamical responses.

We next turn to precipitation intensity, that is, changes in $I_{CP=i}(t)$ in Equation 2. The global mean surface air temperature has increased about 1.1°C since the pre-industrial period (Gillett et al., 2021) with substantially more warming over land (C. Li, Wang, et al., 2021). The atmospheric water-holding capacity increases correspondingly following the Clausius-Clapeyron relation (e.g., Trenberth et al., 2003). The annual mean atmospheric precipitable water has indeed increased during the past decades over China in radiosonde observations and reanalysis, and the increases can be attributed to anthropogenic forcing with greenhouse gases forcing dominating (J. Zhang et al., 2019), consistent with the finding that annual and summer mean temperatures in China have risen substantially due to anthropogenic forcing (e.g., Sun et al., 2021). Summer wet-day precipitable water as represented in the ERA5 reanalysis has also increased (Figure S15 in Supporting Information S1). In the absence of changes in synoptic circulation, precipitation intensity should therefore also increase. In fact, there is evidence of anthropogenic intensification of precipitation extremes in China (e.g., Dong et al., 2021; C. Li, Zwiers, et al., 2021; H. Li et al., 2017; W. Li et al., 2018; Park et al., 2020; J. Wang et al., 2021; Xu et al., 2022; T. Zhou, Ren, et al., 2021). The agreement between this basic thermodynamic law, our estimates of the relatively coherent positive trends of precipitation intensities under given CPs (Figure S16 in Supporting Information S1) and the summer total precipitation trend component contributed by these intensity changes (Figure 1d) indicates that human activities have very likely already affected summer total precipitation in China by increasing precipitation intensity.

The question of anthropogenic influence on precipitation frequency change, that is, changes in $P_{CP=i}(t)$ in Equation 2, which is the dominant factor in the "north-south drying-wetting" pattern, and whether that pattern of change is a consequence of aerosol forcing, remains tenuous. Anthropogenic aerosol burdens in China have increased substantially during the past decades (e.g., Streets et al., 2013). It is thought that aerosols suppress light precipitation through aerosol-cloud interactions (e.g., Y. Wang et al., 2016) and that the historical changes in aerosols may have caused droughts over North China by weakening the East Asia summer monsoon (e.g., Polson et al., 2014; Tian et al., 2018; L. Zhang et al., 2017). In the absence of a strong influence on CP frequency, or secular trends emerging from low-frequency internal variability effects (Figure S17 in Supporting Information S1), it is difficult to imagine that greenhouse gas forcing would lead to the observed pattern of precipitation frequency change. Thus, aerosols emerge as the primary suspect. Nevertheless, our understanding of the climate effects of aerosols is still highly uncertain (e.g., Bellouin et al., 2020) and the adequacy of current climate model simulations in representing the impacts of aerosols on precipitation frequency and monsoon circulation in China, with its complex terrain and heterogenous distribution of aerosol sources, remains a concern (e.g., Z. Li et al., 2019). Thus, further research on the impacts of global warming and aerosol loading on precipitation frequency is crucially needed to better understand whether the complex pattern of summer precipitation trends will continue into future.

4. Discussion and Conclusions

By decomposing the historical trends in summer total precipitation into components due to changes in synoptic CP frequency, daily precipitation frequency, and daily precipitation intensity, we find that the complex pattern of summer total precipitation trends observed in China since the 1960s is overwhelmingly the result of changes in daily precipitation frequency. Changes in precipitation intensity contribute a relatively homogeneous wetting tendency across the country and changes due to synoptic circulation change are found to be weak. Our understanding of the forcing mechanisms for the changes in daily precipitation frequency are still uncertain, although aerosols are suspected. Clarification of this issue will require improvements in our understanding of the role of aerosol-cloud and aerosol-radiation interactions in altering precipitation frequency and in the representation of relevant physical processes in current climate model simulations. Until then, it will remain difficult to determine the relative impacts of anthropogenic forcing and natural variability on the change of precipitation frequency, and thus will remain difficult to project whether the complex pattern of summer precipitation trends in China will continue into the future.

Although climate models appear to be relatively skillful in simulating reanalysis CPs and their frequency of occurrence, some uncertainty in this regard and their ability to simulate long-term CP changes remains. Nevertheless, the trend partition that we have suggested can be useful for sharpening the focus of the search for understanding the causes of complex observed patterns of precipitation change, as we have demonstrated for China. Similar approaches may also prove to be beneficial in other parts of the world where, at a regional scale, our understanding of observed precipitation change remains tenuous. It should, however, be cautioned that the trend decomposition method used in this study considers daily precipitation amounts and CPs on daily time scales. Analyzing seasonal precipitation based on accumulations over periods that are substantially shorter or longer than a day would likely require a different approach to describing the dynamical features responsible for precipitation on those time scales.

Conflict of Interest

The authors declare no conflicts of interest relevant to this study.

Data Availability Statement

The precipitation observations used in this study were acquired from the National Meteorological Information Center of China and can be downloaded from http://101.200.76.197/data/cdcdetail/dataCode/SURF_CLI_CHN_MUL_DAY_V3.0.html. The ERA5 reanalysis data set is available at https://www.ecmwf.int/en/forecasts/dataset/ecmwf-reanalysis-v5. The JRA-55 reanalysis data set is available at https://jra.kishou.go.jp/JRA%2D55/index-%5Fen.html%23jra%2D55. The CMIP6 climate model simulations are available at https://esgf-node.llnl.gov/search/cmip6/.

Acknowledgments
This study was supported by National Key R&D Program of China (2017YFA0603804, 2020YFA0608901) and the National Natural Science Foundation of China (42075026). C.L., Z.J., X.Z., and F.W.Z. designed the study. C.L. and Z.J. formulated the analysis method. M.L. and C.L. conducted the analysis. C.L. and Z.J. wrote the initial draft. All authors interpreted the results and edited the manuscript.

References

Allen, M. R., & Stott, P. A. (2003). Estimating signal amplitudes in optimal fingerprinting: I. Theory. *Climate Dynamics*, *21*, 477–491. https://doi.org/10.1007/s00382-003-0313-9

Bellouin, N., Quaas, J., Gryspeerdt, E., Kinne, S., Stier, P., Watson-Parris, D., et al. (2020). Bounding global aerosol radiative forcing of climate change. *Reviews of Geophysics*, *58*, e2019RG000660. https://doi.org/10.1029/2019RG000660

Cattiaus, J., Douville, H., & Peings, Y. (2013). European temperatures in CMIP5: Origins of present-day biases and future uncertainties. *Climate Dynamics*, *41*, 2889–2907. https://doi.org/10.1007/s00382-013-1731-y

Chou, C., Chen, C., Tan, P., & Chen, K. T. (2012). Mechanisms for global warming impacts on precipitation frequency and intensity. *Journal of Climate*, *25*, 3291–3306. https://doi.org/10.1175/JCLI-D-11-00239.1

Dai, A., Rasmussen, R. M., Liu, C., Ikeda, K., & Prein, A. F. (2020). A new mechanism for warm-season precipitation response to global warming based on convection-permitting simulations. *Climate Dynamics*, *55*, 343–368. https://doi.org/10.1007/s00382-017-3787-6

Ding, Y., Wang, Z., & Sun, Y. (2008). Inter-decadal variation of the summer precipitation in East China and its association with decreasing Asian summer monsoon. Part I: Observation evidence. *International Journal of Climatology*, *28*, 1139–1161. https://doi.org/10.1002/joc.1615

Dong, S., Sun, Y., Li, C., Zhang, X., Min, S. K., & Kim, Y. H. (2021). Attribution of extreme precipitation with updated observations and CMIP6 simulations. *Journal of Climate*, *34*, 871–881. https://doi.org/10.1175/JCLI-D-19-1017.1

Driouech, F., Déqué, M., & Sánchez-Gómez, E. (2010). Weather regimes—Moroccan precipitation link in a regional climate change simulation. *Global and Planetary Change*, *72*, 1–10. https://doi.org/10.1016/j.gloplacha.2010.03.004

Eyring, V., Bony, S., Meehl, G. A., Senior, C. A., Stevens, B., Stouffer, R. J., et al. (2016). Overview of the Coupled Model Intercomparison Project Phase 6 (CMIP6) experimental design and organization. *Geoscientific Model Development*, *9*, 1937–1958. https://doi.org/10.5194/gmd-9-1937-2016

Furrer, E. M., Katz, R. W., Walter, M. D., & Furrer, R. (2010). Statistical modeling of hot spells and heat waves. *Climate Change*, *43*, 191–205. https://doi.org/10.3354/cr00924

Gillett, N. P., Kirchmeier-Young, M., Ribes, A., Shiogama, H., Hegerl, C. G., Knutti, R., et al. (2021). Constraining human contributions to observed warming since the pre-industrial period. *Nature Climate Change*, *11*, 207–212. https://doi.org/10.1038/s41558-020-00965-9

Gong, D., & Ho, C. (2002). Shift in the summer rainfall over the Yangtze River valley in the late 1970s. *Geophysical Research Letters*, *29*, 1436. https://doi.org/10.1029/2001GL014523

Grise, K. M., & Davis, S. M. (2020). Hadley cell expansion in CMIP6 models. *Atmospheric Chemistry and Physics*, *20*, 5249–5268. https://doi.org/10.5194/acp-20-5249-2020

He, C., Zhou, T., Lin, A., Wu, B., Gu, D., Li, C., & Zheng, B. (2015). Enhanced or weakened North Pacific subtropical high under global warming? *Scientific Reports*, *5*, 16771. https://doi.org/10.1038/srep16771

Hersbach, H., Bell, W., Berrisford, P., Horányi, A., Muñoz-Sabater, J., Nicolas, J., et al. (2019). Global reanalysis: Goodbye ERA-Interim, hello ERA5. *ECMWF Newsletter*, *159*, 17–24. https://doi.org/10.21957/vf291hehd7

Hewitson, B. C., & Crane, R. G. (2002). Self-organizing maps: Applications to synoptic climatology. *Climate Research*, *22*, 13–26. https://doi.org/10.3354/cr022013

Horton, D. E., Johnson, N. C., Singh, D., Swain, D. L., Rajaratna, B., & Diffenbaugh, N. S. (2015). Contribution of changes in atmospheric circulation patterns to extreme temperature trends. *Nature*, *522*, 465–469. https://doi.org/10.1038/nature14550

IPCC. (2021). In: In V.Masson-Delmotte (Eds.), *Climate change 2021: The physical science basis. Contribution of Working Group I to the Sixth Assessment Report of the Intergovernmental Panel on Climate Change*. IPCC.

Kendall, M. G. (1975). *Rank correlation methods*. London: Griffin.

Kim, Y., Min, S. K., Son, S., & Choi, J. (2017). Attribution of the local Hadley cell widening in the southern hemisphere. *Geophysical Research Letters*, *44*, 1015–1024. https://doi.org/10.1002/2016GL072353

Kobayashi, S., Ota, Y., Harada, Y., Ebita, A., Moriya, M., Onoda, H., et al. (2015). The JRA-55 reanalysis: General specification and basic characteristics. *Journal of the Meteorological Society of Japan*, *93*, 5–48. https://doi.org/10.2151/jmsj.2015-001

Kohonen, T. (2000). *Self-organizing maps* (3rd ed.).New York: Springer.

Li, C., Wang, Z., Zwiers, F. W., & Zhang, X. (2021). Improving the estimation of human climate influence by selecting appropriate forcing simulations. *Geophysical Research Letters*, *48*, e2021GL095500. https://doi.org/10.1029/2021GL095500

Li, C., Zwiers, F. W., Zhang, X., Li, G., Sun, Y., & Wehner, M. (2021). Changes in annual extremes of daily temperature and precipitation in CMIP6 models. *Journal of Climate*, *34*, 3441–3460. https://doi.org/10.1175/JCLI-D-19-1013.1

Li, H., Chen, H., & Wang, H. (2017). Effects of anthropogenic activity emerging as intensified extreme precipitation over China. *Journal of Geophysical Research: Atmospheres*, *122*, 6899–6914. https://doi.org/10.1002/2016JD026251

Li, W., Jiang, Z., Zhang, X., & Li, L. (2018). On the emergence of anthropogenic signal in extreme precipitation change over China. *Geophysical Research Letters*, *45*, 9179–9185. https://doi.org/10.1029/2018GL079133

Li, Z., Wang, Y., Guo, J., Zhao, C., Cribb, M. C., Dong, X., et al. (2019). East Asian study of tropospheric aerosols and their impact on regional clouds, precipitation, and climate (EAST-AIRCPC). *Journal of Geophysical Research: Atmospheres*, *124*, 13026–13054. https://doi.org/10.1029/2019JD030758

Li, Z., Yan, Z., Tu, K., & Wu, H. (2015). Changes of precipitation and extremes and the possible effect of urbanization in the Beijing metropolitan region during 1960–2012 based on homogenized observations. *Advances in Atmospheric Sciences*, *32*, 1173–1185. https://doi.org/10.1007/s00376-015-4257-x

Lu, E., Zeng, Y., Luo, Y., Ding, Y., Zhao, W., Liu, S., et al. (2014). Changes of summer precipitation in China: The dominance of frequency and intensity and linkage with changes in moisture and air temperature. *Journal of Geophysical Research: Atmospheres*, *119*, 12575–12587. https://doi.org/10.1002/2014jd022456

Ma, S., Zhou, T., Dai, A., & Han, Z. (2015). Observed changes in the distribution of daily precipitation frequency and amount over China from 1960 to 2013. *Journal of Climate*, *28*, 6960–6978. https://doi.org/10.1175/JCLI-D-15-0011.1

Mann, H. B. (1945). Nonparametric tests against trend. *Econometrica*, *13*, 245–259. https://doi.org/10.2307/1907187

Meinshausen, M., Nicholls, Z. R. J., Lewis, J., Gidden, M. J., Vogel, E., Freund, M., et al. (2020). The shared socio-economic pathway (SSP) greenhouse gas concentrations and their extensions to 2500. *Geoscientific Model Development*, *13*, 3571–3605. https://doi.org/10.5194/gmd-13-3571-2020

Menon, S., Hansen, J., Nazarenko, L., & Luo, Y. (2002). Climate effects of black carbon aerosols in China and India. *Science*, *297*, 2250–2253. https://doi.org/10.1126/science.1075159

Paik, S., Min, S., Zhang, X., Donat, M. G., King, A. D., & Sun, Q. (2020). Determining the anthropogenic greenhouse gas contribution to the observed intensification of extreme precipitation. *Geophysical Research Letters*, *47*, e2019GL086875. https://doi.org/10.1029/2019GL086875

Piao, S., Ciais, P., Huang, Y., Shen, Z., Peng, S., Li, J., et al. (2010). The impacts of climate change on water resources and agriculture in China. *Science*, *467*, 43–51. https://doi.org/10.1038/nature09364

Polson, D., Bollasina, M., Hegerl, G. C., & Wilcox, L. J. (2014). Decreased monsoon precipitation in the Northern hemisphere due to anthropogenic aerosols. *Geophysical Research Letters*, *41*, 6023–6029. https://doi.org/10.1002/2014GL060811

Prein, A. F., Holland, G. J., Rasmussen, R. M., Clark, M. P., & Tye, M. R. (2016). Running dry: The U.S. Southwest's drift into a drier climate state. *Geophysical Research Letters*, *43*, 1272–1279. https://doi.org/10.1002/2015GL066727

Ribes, A., Planto, S., & Terray, L. (2013). Application of regularized optimal fingerprinting to attribution. Part I: Method, properties, and idealized analysis. *Climate Dynamics*, *41*, 2817–2836. https://doi.org/10.1007/s00382-013-1735-7

Schar, C., Ban, N., Fischer, M. E., Rajczak, J., Schmidli, J., Frei, C., et al. (2016). Percentile indices for assessing changes in heavy precipitation events. *Climate Change*, *137*, 201–216. https://doi.org/10.1007/s10584-016-1669-2

Sen, P. K. (1968). Estimates of the regression coefficient based on Kendall's tau. *Journal of the American Statistical Association*, *63*, 1379–1389. https://doi.org/10.1080/01621459.1968.10480934

Song, F., & Zhou, T. (2014). The climatology and interannual variability of East Asian summer monsoon in CMIP5 coupled models: Does air-sea coupling improve the simulation? *Journal of Climate*, *15*, 1679–1697. https://doi.org/10.1175/JCLI-D-14-00396.1

Streets, D. G., Shindell, D. T., Lu, Z., & Faluvegi, G. (2013). Radiative forcing due to major aerosol emitting sectors in China and India. *Geophysical Research Letters*, *40*, 4409–4414. https://doi.org/10.1002/grl.50805

Sun, Y., Solomon, S., Dai, A., & Portmann, R. W. (2007). How often will it rain? *Journal of Climate*, *20*, 4801–4818. https://doi.org/10.1175/JCLI4263.1

Sun, Y., Zhang, X., Ding, Y., Chen, D., Qin, D., & Zhai, P. (2021). Understanding human influence on climate change in China. *National Science Review*, *9*, nwab113. https://doi.org/10.1093/nsr/nwab113

Tan, X., Gan, T. Y., Chen, S., Horton, D. E., Chen, X., Liu, B., & Lin, K. (2019). Trends in persistent seasonal-scale atmospheric circulation patterns responsible for seasonal precipitation totals and occurrences of precipitation extremes over Canada. *Journal of Climate*, *32*, 7105–7126. https://doi.org/10.1175/JCLI-D-18-0408.1

Tan, Y., Zwiers, F. W., Yang, S., Li, C., & Deng, K. (2020). The role of circulation and its changes in present and future atmospheric rivers over western North America. *Journal of Climate*, *33*, 1261–1281. https://doi.org/10.1175/JCLI-D-19-0134.1

Tian, F., Dong, B., Robson, J., & Sutton, R. (2018). Forced decadal changes in the East Asian summer monsoon: The roles of greenhouse gases and anthropogenic aerosols. *Climate Dynamics*, *51*, 3699–3715. https://doi.org/10.1007/s00382-018-4105-7

Trenberth, K. E., Dai, A., Rasmussen, R. M., & Parsons, D. B. (2003). The changing character of precipitation. *Bulletin of the American Meteorological Society*, *84*, 1205–1218. https://doi.org/10.1175/BAMS-84-9-1205

Wang, J., Li, C., Zwiers, F. W., Zhang, X., Li, G., Jiang, Z., et al. (2021). On the optimal design of field significance tests for changes in climate extremes. *Geophysical Research Letters*, *48*, e2021GL092831. https://doi.org/10.1029/2021GL092831

Wang, Y., Ma, P., Jiang, J. H., Su, H., & Rasch, P. J. (2016). Toward reconciling the influence of atmospheric aerosols and greenhouse gases on light precipitation changes in eastern China. *Journal of Geophysical Research: Atmospheres*, *121*, 5878–5887. https://doi.org/10.1002/2016JD024845

Xu, X., Chen, H., & Wang, H. (2022). Detectable human influence on changes in precipitation extremes across China. *Earth's Future*, *10*, e2021EF002409. https://doi.org/10.1029/2021EF002409

Zhai, P., Zhang, X., Wan, H., & Pan, X. (2004). Trends in total precipitation and frequency of daily precipitation extremes over China. *Journal of Climate*, *17*, 1096–1108. https://doi.org/10.1175/JCLI-3318.1

Zhang, J., Zhao, T., Dai, A., & Zhang, W. (2019). Detection and attribution of atmospheric precipitable water changes since the 1970s over China. *Scientific Reports*, *9*, 17609. https://doi.org/10.1038/s41598-019-54185-z

Zhang, L., Wu, P., & Zhou, T. (2017). Aerosol forcing of extreme summer drought over North China. *Environmental Research Letters*, *12*, 034020. https://doi.org/10.1088/1748-9326/aa5fb3

Zhang, R. (2015). Changes in East Asian summer monsoon and summer rainfall over eastern China during recent decades. *Science Bulletin*, *60*, 1222–1224. https://doi.org/10.1007/s11434-015-0824-x

Zhou, B., Zhai, P., & Chen, Y. (2020). Contribution of changes in synoptic-scale circulation patterns to the past summer precipitation regime shift in eastern China. *Geophysical Research Letters*, *47*, e2020GL087728. https://doi.org/10.1029/2020GL087728

Zhou, B., Zhai, P., Tett, S. B., & Lott, F. C. (2021). Detectable anthropogenic changes in daily-scale circulation driving summer rainfall shifts over eastern China. *Environmental Research Letters*, *16*, 074044. https://doi.org/10.1088/1748-9326/ac0f28

Zhou, T., Ren, L., & Zhang, W. (2021). Anthropogenic influence on extreme Meiyu rainfall in 2020 and its future risk. *Science China Earth Sciences*, *64*, 1633–1644. https://doi.org/10.1007/s11430-020-9771-8